Reactions $K^-p \to \Sigma^-\pi^+$ and $K^-p \to \Sigma^+\pi^-$ in the momentum range from 220 to 470 MeV/c

R. O. Bangerter,* M. Alston-Garnjost, A. Barbaro-Galtieri, T. S. Mast, F. T. Solmitz, and R. D. Tripp
Lawrence Berkeley Laboratory, University of California, Berkeley, California 94720
(Received 28 January 1980)

We present the analysis of 64 000 $K^-p \to \Sigma^-\pi^+$ and 89 000 $K^-p \to \Sigma^+\pi^-$ events obtained with the Berkeley 25-in. hydrogen bubble chamber. Total cross sections and Legendre-polynomial expansion coefficients describing the differential cross sections and polarizations are presented in 10-MeV/c momentum intervals extending from 220 to 470 MeV/c. This paper completes the series devoted to all K^-p final states in this momentum range.

I. INTRODUCTION

This paper is one of a series reporting a high-statistics study of the K^-p interaction in the momentum region from 220 to 470 MeV/c.[1] The experiment was performed at Lawrence Berkeley Laboratory using the 25-in. hydrogen bubble chamber. The exposure consisted of 1.3×10^6 pictures, resulting in the path-length distribution shown in Fig. 1. Most of the experiment was run with a beam momentum near 390 MeV/c, corresponding to the energy required to produce $\Lambda(1520)$. The interference of $\Lambda(1520)$ with the large S-wave background creates highly polarized $\Sigma^\pm$ that have previously been analyzed to provide information on the $\Sigma^\pm$ decay parameters.[2-6] Although the entire data sample was used to obtain the decay parameters reported in Refs. 4 and 6, this paper is the first detailed publication of polarizations and angular distributions obtained from the entire sample.

In Sec. II we describe the experimental procedures used to obtain the data and discuss the problems of biases and ambiguities. Section III contains a description of the fitting procedures used to obtain cross sections and Legendre-polynomial coefficients describing the data, and in Sec. IV we present our results.

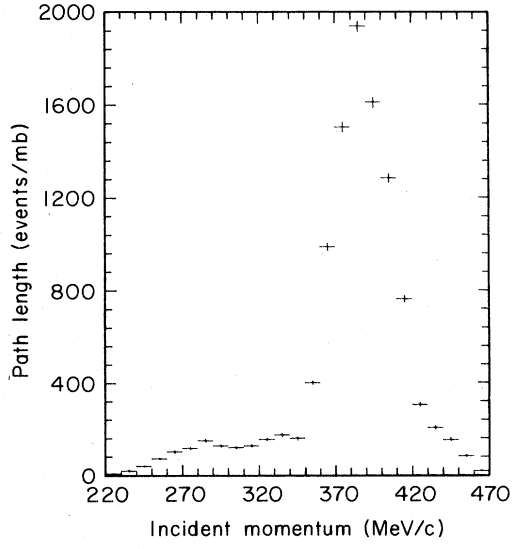

FIG. 1. Path length (events/mb) as a function of K^- momentum (MeV/c).

II. EXPERIMENTAL PROCEDURES

A. Scanning

The film was scanned for all topologies. In particular, the scanners were asked to record all examples of the following reaction sequences:

$$K^-p \to \Sigma^-\pi^+, \quad \Sigma^- \to n\pi^-;$$
$$K^-p \to \Sigma^+\pi^-, \quad \Sigma^+ \to p\pi^0;$$
$$K^-p \to \Sigma^+\pi^-, \quad \Sigma^+ \to n\pi^+.$$

For brevity we will refer to these as Σ^-_-, Σ^+_0, and Σ^+_+ channels, where the subscript refers to the charge of the decay pion.

There are two difficulties in selecting the above event types. The first results from non-Σ events that are topologically similar to the true events. Examples of this are the reactions $K^-p \to K^-p$ followed by $pp \to pp$, where one of the scattered protons is too short to be visible and $K^-p \to K^-p$ followed by $K^- \to \mu^-\bar{\nu}$ (or $K^- \to \pi^-\pi^0$). After scanning, measuring, and fitting, we estimate that all possible non-Σ channels contribute a contamination of much less than 1% and can be neglected.

The second difficulty is more serious and results from the ambiguity between Σ^+_0 and Σ^+_+ events. Because the decay asymmetry parameter α_0 (for Σ^+_0) is nearly -1, whereas α_+ (for Σ^+_+) is nearly zero,[6] it is important to distinguish Σ^+_0 from Σ^+_+ in order to measure the polarization, the asymmetry parameters, and the branching fraction reliably.

The cameras are located in such a way that the projections seen by the scanners closely approximate the projection on the horizontal plane of the bubble chamber. The momentum of the decay pion or proton is typically several hundred MeV/c so that the proton ionizes much more heavily than the pion. For those events in which the charged

decay product makes a dip angle (λ) of less than 50° with respect to the horizontal plane, the scanners are able to distinguish Σ^+_+ and Σ^+_0 with better than 95% reliability. All tracks having $|\lambda| > 50°$ appear rather dark, making it more difficult to distinguish differences in ionization and reducing the scanners's reliability to somewhat greater than 75%. Resolution of this scanning ambiguity is discussed in detail in Sec. IIC.

In addition to the ambiguity problem, scanners will have difficulty detecting events with very short Σ tracks or events having a small projected angle between the Σ and its charged decay product. Of course, the scanners will even fail to detect some fraction of the highly visible events. To investigate these biases we have scanned 38% of our film twice and 7% three times. Using an extension of the method of Derenzo and Hildebrand,[7] we have established the scanning efficiency as a function of projected Σ-secondary angle and projected Σ track length. We found that the scanning efficiency dropped precipitously for projected Σ decay lengths $\lesssim 0.15$ cm, projected decay angles $\lesssim 8°$, and projected secondary track lengths $\lesssim 0.3$ cm.

We have also investigated short-length Σ losses by weighting our events by $e^{t/\tau}$ and plotting the distribution as a function of projected length. Here, t is proper time and τ is the mean life. Neglecting the small fraction of events decaying outside the bubble chamber, this distribution should be flat. Thus it provides a direct measure of the relative scanning efficiency as a function of projected Σ track length. The two methods are in reasonable agreement and a freehand curve representing the scanning efficiency for the three event types as a function of projected length is shown in Fig. 2.

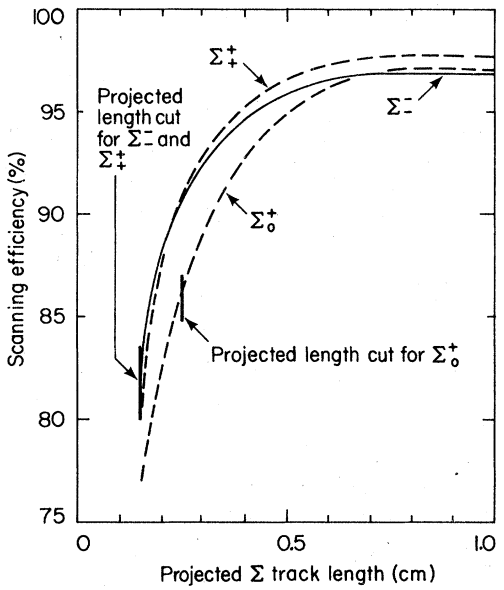

FIG. 2. Scanning efficiency as a function of Σ track length projected on the horizontal plane. These efficiencies are for events having a projected decay angle greater than 12°. Events having projected decay angles between 8° and 12° have somewhat lower efficiencies. Events having lengths shorter than the indicated cuts were not used for determining the angular distributions.

B. Measuring and fitting

The scanners make a crude determination of an event's position using a projected grid. This measurement is used to determine if an event lies in a measurement fiducial volume chosen small enough to ensure that the event has adequate track length for meaningful measurements. Events lying in this fiducial volume have been measured on the Spiral Reader and/or Franckenstein measuring machines. Geometric reconstruction and kinematic analysis were performed using programs TVGP and SQUAW.

Those events for which geometric reconstruction failed or that did not give an adequate (confidence level ≥ 0.01) kinematic fit were repeatedly remeasured to ensure that the failure was not the result of measurement errors. A certain failure rate is unavoidable because of tracks obscured by other tracks in the bubble chamber, large-angle scattering fluctuations, and very short tracks. Events have also been lost for a variety of other reasons such as imperfections in data tapes. We assume that the small residue lost will not bias the angular distributions or decay asymmetries and have applied corrections of 1.05, 1.06, and 1.06, respectively, to obtain the Σ^-, Σ^+_0, and Σ^+_+ cross sections given in Sec. IV. We estimate that these correction factors are accurate to about 1%.

C. Ambiguities between Σ^+_0 and Σ^+_+

As noted above, the most difficult contamination problem results from the ambiguity between Σ^+_0 and Σ^+_+. There are three categories of information that allow us to distinguish these decay modes.

(1) Kinematics. Only about 19% of all Σ^+ decays fit both Σ^+_+ and Σ^+_0. Even where both mass hypotheses fit, one will be preferred on the basis of the relative confidence levels.

(2) Ionization and range information. The momentum of the pion or proton is typically several hundred MeV/c so that the proton ionizes much more heavily than the pion. Discrimination between the two Σ^+ decay modes is made in the following ways. (a) In most cases the scanners are able to make a reliable judgment about ionization. This is discussed in Sec. IIA. (b) About half of our events were measured on the Spiral Reader.

The Spiral Reader automatically measures track darkness and this information is used to calculate a χ^2 for each mass hypothesis. (c) The range of a proton is much smaller than that of a pion having equal momentum. Many protons stop in the bubble chamber. This stopping-proton information alone is sufficient to reduce the ambiguities from 19% to 7%. (d) Furthermore, if the fitted momentum of the proton hypothesis gives a range significantly smaller than the measured length of the track, the proton hypothesis may be rejected. (e) Because of its greater energy loss, the radius of curvature of a proton decreases more rapidly than that of a pion. In some cases this difference gives an unambiguous mass determination in the process of geometric track reconstruction. In all cases, TVGP computes a track χ^2 for both mass hypotheses.

(3) Expected decay distribution. Let $\hat{\Sigma}$ and $\hat{v}$ be unit vectors along the Σ and charged decay-product directions, respectively. Although both Σ_+^+ and Σ_0^+ events are uniformly distributed in $\hat{\Sigma}\cdot\hat{v}$ in the Σ rest frame, the laboratory distributions are quite dissimilar. An *a priori* probability for each hypothesis may be assigned on the basis of $\hat{\Sigma}\cdot\hat{v}$ as measured in the laboratory.

Those events that are unambiguously fitted by SQUAW are checked for consistency with the range-momentum conditions of 2c and 2d, above. If consistent, these events are considered to be truly unambiguous. For ambiguous events, all of the available information described above is used to form a probability ratio for the Σ_0^+ and Σ_+^+ hypotheses. Not all of the information is truly independent, and a rigorous calculation of the ratio is probably impossible. Therefore, we have tried to calculate the ratio in a way that underestimates the value of the information. Nevertheless, in nearly all cases one hypothesis is very strongly preferred. We calculate the contamination of each channel is <0.4%. Additional details of this selection procedure are given in Ref. 4.

III. FITS TO CROSS SECTIONS, ANGULAR DISTRIBUTIONS, AND POLARIZATIONS

A. Cuts and corrections

Not all of the measured events were used in this analysis. The measuring fiducial volume described in Sec. IIB was applied using rather crude measurements made on the scanning projector. A more restrictive fiducial volume constraint was imposed on the events using the measured coordinates of the Σ production vertex. The Σ decay vertex was required to be in a somewhat larger fiducial volume. These same fiducial volume constraints were also applied to the other event types described in this series of papers.[1]

The events used for the determination of cross sections and angular distributions were subjected to additional cuts on the projected track length of, and projected angle between, the Σ and the charged decay product. As explained above, all projections refer to the horizontal plane and closely approximate the projections seen by the scanners.

For the Σ_-^- and Σ_+^+ reactions, events having a projected Σ track length less than 0.15 cm are rejected. If a Σ^- decays within 0.1 cm of the end of its range, it is rejected to facilitate the correction for $\Sigma^- p \to \Lambda n$, where the Σ^- is at rest. Because there is typically much less change in track darkness and angle for the Σ_0^+ decay, these decays are more difficult to detect and we demand a minimum projected length of 0.25 cm.

For all three event types we require a projected Σ secondary angle of at least 8° and a projected secondary track length of at least 0.3 cm. The number of events in the fiducial volumes and the number satisfying the length and angle cuts are given in Table I.

It can be shown that the events not surviving the length and angle cuts result in an unbiased determination of the product of the decay parameter and polarization αP.[4] These events are retained for part of the analysis, as will be described below.

The length and angle cuts have a large effect on the angular distribution. For a given beam momentum and production cosine ($\cos\theta = \hat{K}\cdot\hat{\pi}$), one can calculate the fraction of events surviving the cuts by performing the appropriate integrals over all of the remaining variables. These variables are production aximuth, Σ decay length, and the two angles specifying the Σ decay. We have performed these integrals numerically, even taking into account such effects as Σ energy loss. Examples of the resulting detection efficiency as a function of $\cos\theta$ are shown in Fig. 3. These curves assume that the scanning (and mea-

TABLE I. The number of events in the fiducial volumes and the number satisfying the length and angle cuts.

Event type	Events in fiducial volumes	Events surviving length and angle cuts
Σ_-^-	64 059	53 643
Σ_0^+	42 253	30 562
Σ_+^+	47 090	38 207

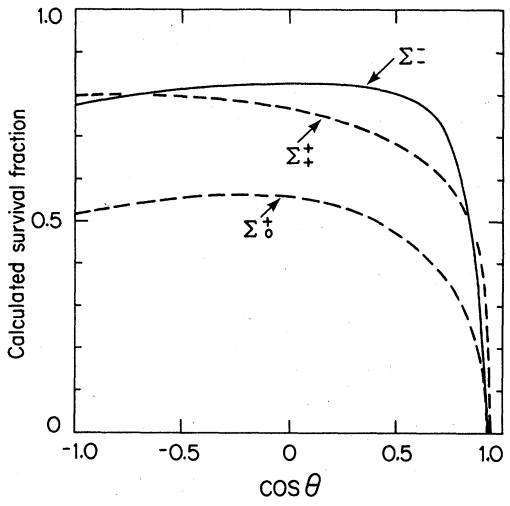

FIG. 3. Calculated fraction of events surviving the projected length and angle cuts as a function of production cosine. These curves correspond to a beam momentum of 385 MeV/c. Despite the longer mean life for Σ^-, its curve falls below the curve for Σ^+_+ because of the $\Sigma^- p \to \Lambda n$ correction described in the text.

suring) efficiency is 100% for those events surviving the cuts. Figure 2 illustrates that this is not the case. There is still some dependence of scanning efficiency on the geometric properties of the event. Moreover, there is some probability that a Σ produced inside the production fiducial volume will decay outside of the decay fiducial volume. Escape corrections are calculated to account for this effect.

B. Maximum-likelihood fitting

For our analysis we have divided the events into 25 momentum bins having widths of 10 MeV/c and covering the range from 220 to 470 MeV/c. For each momentum bin we expand the probability distribution function as follows:

$$R(\theta,\beta;\vec{A}) = \frac{d^2I}{d\cos\theta\, d\cos\beta} = \frac{A_0}{2}\left[1 + \sum_{l=1}^{L} \frac{A_l}{A_0} P_l(\cos\theta) + \cos\beta \sum_{l=1}^{l} \frac{B_l}{A_0} P_l^1(\cos\theta)\right],$$

where β is the angle between the production normal $(\vec{K}\times\vec{\pi})$ and the decay nucleon as measured in the Σ rest frame. Functions P_l and P_l^1 are the Legendre polynomials and $\vec{A}$ is the vector $(A_0, A_1/A_0, \ldots, A_L/A_0, B_1/A_0, \ldots, B_L/A_0)$. The polarization of the Σ is directed along the production normal and its sign and magnitude are given by

$$P = \frac{1}{\alpha} \sum_{l=1}^{L} B_l P_l^1(\cos\theta) \Big/ \sum_{l=0}^{L} A_l P_l(\cos\theta).$$

The sign convention of α is that of the Particle Data Group[6] and has been used in all of the earlier papers in this series. We emphasize that the expansion coefficients describe αP—not just P—since αP is the measurable quantity.

For statistical efficiency we choose to obtain $\vec{A}$ using the maximum-likelihood method. If the detection efficiency were 100% we could write the likelihood function as

$$\mathcal{L}(\vec{A}) = \frac{1}{N!} e^{-2A_0} \sum_{i=1}^{N} R(\theta_i,\beta_i;\vec{A}),$$

where N is the total number of events. A little rearrangement shows that this is simply the product of a Poisson distribution for the total number of events $(2A_0)$ times the likelihood function for the angular distribution.[8] Neglecting terms independent of $\vec{A}$, we write the logarithm of the likelihood function as

$$W(\vec{A}) = -2A_0 + \sum_{i=1}^{N} \ln R(\theta_i,\beta_i;\vec{A}).$$

Because the detection efficiency is not 100% one could consider modifying $W(\vec{A})$ by introducing weights on the individual events so that

$$W(\vec{A}) = -2A_0 + \sum_{i=1}^{N} w_i \ln R(\theta_i,\beta_i;\vec{A}),$$

where $w_i = f/(\epsilon_i s_i d_i)$. The quantity f is the correction factor for lost and failing events described in Sec. II, and ϵ_i, s_i, and d_i are, respectively, the scanning efficiency given in Fig. 2, the survival rate given in Fig. 3, and the probability that the decay vertex of the ith event lies within the decay fiducial volume. There is a problem with this approach. The weights are infinite for $s = 0$. This problem could be solved by placing a cut on $\cos\theta$ and making an appropriate modification to the likelihood function. In preliminary analyses, we made a cut in $\cos\theta$; however, unless the cut is quite severe, eliminating many events having $\cos\theta$ close to 1, there is a wide variation in the magnitude of w_i for different events. Even if few events were eliminated by the $\cos\theta$ cut, the use of highly variable weights is statistically inefficient.[8]

If we temporarily neglect f, ϵ, and d, we can replace R by $R' = Rs(\cos\theta)$. The expected number of events is no longer given by $2A_0$, but by

$$\int R(\theta,\beta;\vec{A})s(\cos\theta)d\cos\theta\, d\cos\beta = A_0\left(G_0+\sum_{l=1}^{L}\frac{A_l}{A_0}G_l\right),$$

where $G_l=\int P_l(\cos\theta)s(\cos\theta)d\cos\theta$. Dropping terms independent of $\vec{A}$, the logarithm of the likelihood function becomes

$$W_1(\vec{A}) = -A_0\left(G_0+\sum_{l=1}^{L}\frac{A_l}{A_0}G_l\right) + \sum_{i=1}^{N} w_i \ln R(\theta_i,\beta_i;\vec{A}),$$

where $w_i=f/(\epsilon_i d_i)$ is now quite close to unity for all events and can be applied with only a small penalty in statistical efficiency. The G_l have been calculated for each momentum.

Since the events rejected by the cuts give an unbiased maximum-likelihood estimate of αP, we can write the logarithm of the likelihood function for these events as

$$W_2(\vec{A}) = \sum_{i=N+1}^{M} \ln\left[1+\cos\beta_i\,\frac{\sum_{l=1}^{L}\frac{B_l}{A_0}P_l^1(\cos\theta_i)}{1+\sum_{l=1}^{L}\frac{A_l}{A_0}P_l(\cos\theta_i)}\right] \equiv \sum_{i=N+1}^{M}\ln Q(\beta_i,\theta_i;\vec{A}),$$

where the sum is over the $M-N$ events not surviving the projected length and angle cuts. The total function for the entire set of data becomes

$$W_T(\vec{A}) = W_1(\vec{A}) + W_2(\vec{A}).$$

Values of $\vec{A}$ for each momentum and channel are obtained by maximizing W_T with respect to $\vec{A}$ with the computer. The error matrix $\underline{E}$ for $\vec{A}$ is calculated by the computer assuming W_T is quadratic in $\vec{A}$ near the maximum. The expression used for $\underline{E}$ is

$$\underline{E}=\underline{D}^{-1}\underline{H}\underline{D}^{-1},$$

where

$$H_{jk}=\sum_{i=1}^{N}\left(\frac{w_i}{R_i}\right)^2\frac{\partial R_i}{\partial A_j}\frac{\partial R_i}{\partial A_k}+\sum_{i=N+1}^{M}\frac{1}{Q_i^2}\frac{\partial Q_i}{\partial A_j}\frac{\partial Q_i}{\partial A_k}$$

and

$$D_{jk}=-\frac{\partial^2 W_T}{\partial A_j\,\partial A_k}.$$

This expression for $\underline{E}$ is an extension of the results given in Ref. 8 and can be derived by expanding W_T to second order about the true values of $\vec{A}$. At those momenta having few events, the quadratic approximation to W_T becomes poor and we experienced some difficulties with the maximum-likelihood method. For this reason we employed the method of least squares at 225 to 255 MeV/c and at 465 MeV/c.

C. Additional corrections

Before performing kinematic fitting, the momentum of the K^- beam particle was determined by averaging the measured momentum with an expected momentum determined by fitting a large number of τ decays ($K^-\to\pi^-\pi^-\pi^+$). The expected momentum was different for each of 24 beam settings. This averaging procedure is advantageous in reducing ambiguities resulting from short beam tracks having large measurement uncertainties; however, the fitted beam momentum is systematically pulled toward the expected value and thus distorts the fitted momentum distribution. Even if this averaging procedure had not been employed, distortion would occur simply because of the uncertainty in the fitted momentum of the beam track. In either case, a given momentum

TABLE II. Path length at each of the 25 momenta studied in this experiment.

Momentum (MeV/c)	Path length (events/mb)
225	7.4 ± 1.1
235	20.3 ± 1.8
245	40.5 ± 2.6
255	72.5 ± 3.6
265	102.1 ± 4.4
275	116.3 ± 4.8
285	151.2 ± 5.5
295	128.6 ± 5.1
305	119.2 ± 4.8
315	128.4 ± 5.0
325	115.6 ± 5.5
335	174.0 ± 5.9
345	159.1 ± 5.7
355	400.7 ± 9.3
365	988.5 ± 16.2
375	1503.0 ± 20.9
385	1937.4 ± 23.4
395	1609.1 ± 21.1
405	1284.0 ± 19.3
415	763.2 ± 14.1
425	306.0 ± 8.5
435	204.6 ± 7.1
445	153.1 ± 6.3
455	81.9 ± 4.5
465	18.7 ± 2.2

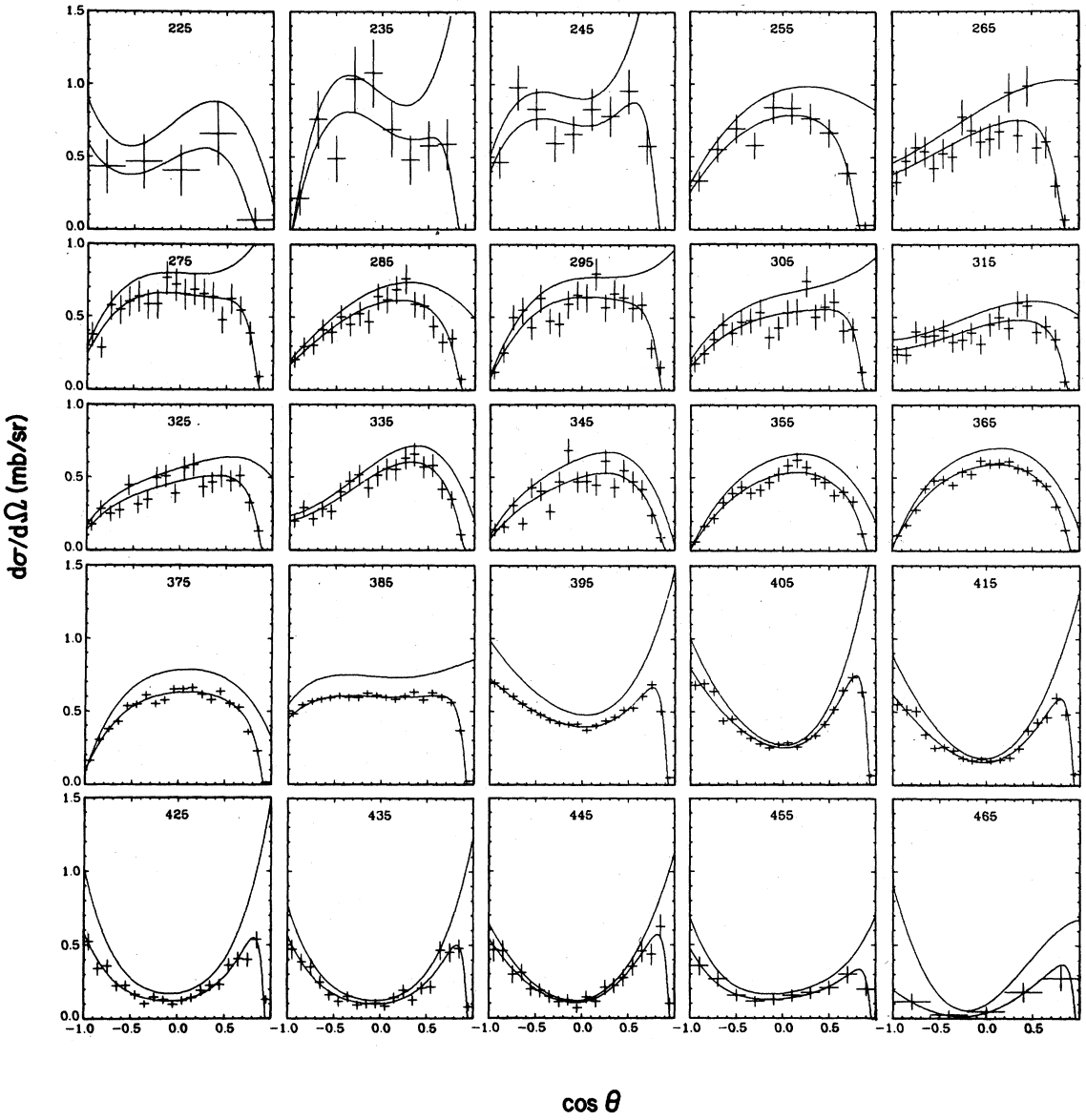

FIG. 4. Differential cross section for $\Sigma^- \pi^+$ as a function of production cosine. The upper curve gives the corrected value of $d\sigma/d\Omega$ as calculated from the data in Table III. The lower curve is the curve that was actually fitted to the data.

bin contains events that truly belong in neighboring bins. It became apparent that the distortion was serious when we compared cross sections determined using different beam settings. We have derived a rather elaborate procedure to correct for this effect.[9] At the lowest and highest momenta these corrections are large and we have increased the fitted uncertainty in the cross sections at 225, 235, and 465 MeV/c to reflect the uncertainty introduced by the corrections.

In fact, any such correction procedure must express the corrected values of $\vec{A}$ in terms of the uncorrected values from several adjacent momentum bins so that the $\vec{A}$ coefficients at a given momentum are statistically correlated with those for other momenta. We ignore these correlations in this paper although we have developed a method for dealing with them in doing partial-wave analyses.[9] This method is quite complex and, in our judgment, introducing such complexity into a partial-wave analysis would not be justified by significantly improved results.

TABLE III. Cross sections, Legendre-polynomial coefficients, and errors for Σ^-.

p_K (MeV/c)	σ (mb)	A_1/A_0	A_2/A_0	A_3/A_0	A_4/A_0	B_1/A_0	B_2/A_0	B_3/A_0	B_4/A_0	$\frac{d\sigma}{d\Omega}(0)$ (mb/sr)	$\frac{d\sigma}{d\Omega}(\pi)$ (mb/sr)
225	8.73	−0.025	−0.235	−0.491		0.135	−0.346	−0.157		0.173	0.891
	±3.26	±0.818	±1.051	±1.234		±0.357	±0.285	±0.254		±2.038	±0.741
235	13.01	0.578	0.203	0.700		−0.392	−0.230	−0.126		2.568	−0.077
	±2.26	±0.277	±0.420	±0.298		±0.147	±0.119	±0.076		±1.257	±0.238
245	14.80	0.628	0.469	0.405		−0.099	−0.165	0.001		2.948	0.513
	±1.63	±0.159	±0.220	±0.209		±0.111	±0.099	±0.082		±0.844	±0.211
255	10.47	0.272	−0.319	0.033		0.012	0.013	0.142		0.823	0.313
	±0.91	±0.150	±0.234	±0.204		±0.098	±0.077	±0.062		±0.493	±0.131
265	10.16	0.394	−0.086	−0.048		−0.100	−0.131	−0.045		1.019	0.459
	±0.74	±0.119	±0.173	±0.162		±0.076	±0.059	±0.051		±0.376	±0.116
275	9.94	0.335	−0.026	0.253		−0.009	−0.083	0.030		1.235	0.304
	±0.66	±0.100	±0.147	±0.130		±0.075	±0.059	±0.048		±0.308	±0.089
285	7.42	0.293	−0.408	−0.054		−0.058	−0.053	0.009		0.491	0.208
	±0.46	±0.094	±0.145	±0.135		±0.077	±0.057	±0.045		±0.208	±0.070
295	8.73	0.413	−0.231	0.219		0.181	0.050	−0.003		0.973	0.095
	±0.55	±0.092	±0.147	±0.116		±0.073	±0.057	±0.049		±0.252	±0.063
305	7.89	0.434	−0.104	0.125		0.035	0.045	0.075		0.914	0.211
	±0.51	±0.101	±0.154	±0.140		±0.080	±0.062	±0.050		±0.250	±0.078
315	6.41	0.272	−0.153	−0.109		−0.193	0.072	0.103		0.515	0.349
	±0.42	±0.113	±0.164	±0.161		±0.081	±0.062	±0.053		±0.215	±0.081
325	6.45	0.346	−0.263	−0.035	−0.084	−0.060	0.095	−0.001	0.008	0.495	0.175
	±0.42	±0.112	±0.182	±0.196	±0.172	±0.073	±0.055	±0.047	±0.040	±0.326	±0.075
335	6.38	0.302	−0.523	−0.338	−0.047	−0.059	0.005	0.056	0.005	0.200	0.236
	±0.37	±0.084	±0.140	±0.154	±0.142	±0.071	±0.050	±0.042	±0.035	±0.230	±0.072
345	6.10	0.152	−0.725	−0.222	−0.127	−0.118	−0.039	−0.104	−0.007	0.038	0.106
	±0.35	±0.094	±0.154	±0.174	±0.157	±0.080	±0.055	±0.043	±0.038	±0.242	±0.066
355	6.14	0.233	−0.721	−0.050	−0.072	−0.065	0.004	0.012	−0.027	0.191	0.012
	±0.23	±0.056	±0.091	±0.106	±0.088	±0.050	±0.035	±0.029	±0.025	±0.147	±0.023
365	6.59	0.157	−0.743	−0.038	−0.108	0.012	0.021	0.014	0.008	0.141	0.016
	±0.16	±0.031	±0.046	±0.053	±0.049	±0.030	±0.021	±0.017	±0.014	±0.078	±0.018
375	7.89	0.142	−0.577	0.045	−0.101	0.030	0.036	0.008	−0.005	0.319	0.085
	±0.15	±0.024	±0.035	±0.040	±0.039	±0.022	±0.016	±0.013	±0.011	±0.072	±0.023
385	9.32	0.102	−0.009	0.103	−0.041	0.003	0.040	0.017	0.007	0.856	0.553
	±0.15	±0.022	±0.030	±0.033	±0.035	±0.017	±0.013	±0.011	±0.010	±0.076	±0.033
395	8.95	0.188	0.689	0.160	0.036	−0.008	0.046	0.006	0.005	1.477	0.981
	±0.16	±0.026	±0.033	±0.038	±0.041	±0.018	±0.016	±0.013	±0.012	±0.090	±0.044
405	7.63	0.364	1.174	0.248	0.081	0.008	0.057	0.001	0.001	1.741	0.997
	±0.17	±0.031	±0.036	±0.044	±0.047	±0.020	±0.018	±0.015	±0.014	±0.096	±0.048
415	6.12	0.324	1.254	0.130	0.005	0.006	0.025	−0.029	−0.035	1.320	0.878
	±0.17	±0.047	±0.053	±0.065	±0.070	±0.030	±0.029	±0.023	±0.020	±0.109	±0.057
425	5.75	0.394	1.445	0.129	0.274	0.039	0.079,	0.073	0.050	1.484	1.005
	±0.23	±0.078	±0.085	±0.107	±0.112	±0.049	±0.048	±0.039	±0.034	±0.163	±0.092
435	4.53	0.459	1.506	0.191	0.263	−0.061	−0.033	0.061	0.018	1.232	0.764
	±0.26	±0.101	±0.111	±0.138	±0.148	±0.066	±0.064	±0.050	±0.047	±0.176	±0.098
445	4.56	0.526	1.374	0.156	0.056	−0.077	−0.004	−0.046	−0.020	1.130	0.635
	±0.32	±0.108	±0.119	±0.148	±0.162	±0.069	±0.067	±0.053	±0.047	±0.190	±0.103
455	3.83	0.118	1.047	−0.092	0.217	−0.202	−0.012	−0.051	0.058	0.699	0.683
	±0.35	±0.166	±0.205	±0.242	±0.277	±0.110	±0.101	±0.081	±0.075	±0.228	±0.155
465	4.26	0.267	1.384	−0.596	−0.056	−0.013	0.512	−0.122	0.116	0.678	0.901
	±1.09	±0.423	±0.667	±0.840	±1.087	±0.320	±0.316	±0.212	±0.220	±0.933	±0.495

D. Calculation of the cross sections

The total cross section for a given channel is given by

$$\sigma = 2A_0/t\,,$$

where t is the path length plotted in Fig. 1 and given numerically in Table II. The values of t

TABLE IV. Cross sections, Legendre-polynomial coefficients, and errors for Σ^+

p_K (MeV/c)	σ (mb)	A_1/A_0	A_2/A_0	A_3/A_0	A_4/A_0	B_1/A_0	B_2/A_0	B_3/A_0	B_4/A_0	$\frac{d\sigma}{d\Omega}(0)$ (mb/sr)	$\frac{d\sigma}{d\Omega}(\pi)$ (mb/sr)
225	13.49	−1.133	0.356	−0.518		0.217	0.336	0.016		−0.316	3.229
	±4.24	±0.868	±0.778	±1.085		±0.596	±0.447	±0.616		±2.487	±1.619
235	15.05	−0.590	0.285	−0.528		−0.027	−0.124	0.129		0.201	2.878
	±2.18	±0.300	±0.317	±0.472		±0.479	±0.417	±0.368		±1.108	±0.718
245	15.03	−0.489	0.157	0.227		−0.227	0.144	0.038		1.072	1.697
	±1.49	±0.187	±0.212	±0.251		±0.175	±0.130	±0.122		±0.687	±0.390
255	12.36	−0.274	0.191	0.024		−0.105	0.393	0.190		0.925	1.417
	±1.01	±0.145	±0.171	±0.203		±0.116	±0.091	±0.072		±0.465	±0.233
265	13.44	−0.198	−0.040	−0.162		−0.411	0.050	−0.160		0.643	1.412
	±0.86	±0.089	±0.111	±0.120		±0.101	±0.082	±0.066		±0.270	±0.183
275	13.23	−0.351	0.093	0.124		−0.287	0.076	0.041		0.912	1.389
	±0.81	±0.097	±0.118	±0.132		±0.091	±0.071	±0.059		±0.319	±0.179
285	10.20	−0.405	−0.163	0.275		−0.396	0.190	0.025		0.574	0.785
	±0.61	±0.081	±0.106	±0.118		±0.082	±0.062	±0.056		±0.208	±0.124
295	12.46	−0.180	0.079	0.195		−0.447	0.201	−0.058		1.085	1.055
	±0.72	±0.084	±0.107	±0.114		±0.085	±0.069	±0.059		±0.268	±0.144
305	11.16	−0.327	0.113	0.172		−0.626	0.321	0.015		0.851	1.126
	±0.63	±0.096	±0.116	±0.135		±0.090	±0.070	±0.059		±0.264	±0.161
315	10.73	−0.108	−0.074	0.153		−0.467	0.138	0.070		0.828	0.752
	±0.60	±0.081	±0.105	±0.118		±0.088	±0.069	±0.059		±0.220	±0.122
325	10.64	−0.240	0.116	0.237	0.036	−0.564	0.166	−0.003	−0.070	0.973	0.978
	±0.58	±0.084	±0.105	±0.117	±0.121	±0.074	±0.061	±0.052	±0.048	±0.307	±0.145
335	9.85	−0.112	0.227	0.354	0.054	−0.435	0.213	−0.036	0.019	1.193	0.814
	±0.55	±0.080	±0.100	±0.111	±0.119	±0.071	±0.059	±0.051	±0.046	±0.287	±0.127
345	10.93	−0.281	0.243	0.135	0.067	−0.708	0.278	−0.041	0.036	1.012	1.266
	±0.53	±0.084	±0.102	±0.116	±0.127	±0.079	±0.064	±0.055	±0.047	±0.299	±0.168
355	10.55	−0.364	0.323	0.314	0.040	−0.547	0.416	−0.014	0.006	1.102	1.187
	±0.34	±0.054	±0.064	±0.071	±0.080	±0.047	±0.038	±0.033	±0.029	±0.185	±0.106
365	10.37	−0.354	0.545	0.333	−0.062	−0.555	0.480	−0.075	−0.021	1.207	1.241
	±0.25	±0.035	±0.039	±0.044	±0.049	±0.027	±0.023	±0.020	±0.018	±0.117	±0.066
375	12.44	−0.353	1.013	0.264	−0.040	−0.528	0.470	−0.147	−0.008	1.865	2.041
	±0.23	±0.028	±0.028	±0.033	±0.038	±0.020	±0.019	±0.016	±0.013	±0.110	±0.069
385	13.85	−0.385	1.547	0.016	−0.048	−0.414	0.260	−0.148	−0.007	2.348	3.161
	±0.22	±0.024	±0.021	±0.027	±0.030	±0.016	±0.017	±0.012	±0.011	±0.102	±0.075
395	13.38	−0.227	1.661	−0.108	−0.071	−0.337	−0.057	−0.125	0.001	2.400	3.115
	±0.22	±0.027	±0.024	±0.031	±0.034	±0.019	±0.020	±0.015	±0.013	±0.112	±0.081
405	10.76	−0.195	1.387	−0.308	−0.047	−0.365	−0.334	−0.098	−0.021	1.572	2.435
	±0.23	±0.029	±0.029	±0.037	±0.039	±0.022	±0.022	±0.017	±0.015	±0.100	±0.078
415	10.16	−0.231	1.061	−0.436	−0.044	−0.420	−0.378	−0.083	0.004	1.092	2.170
	±0.24	±0.040	±0.043	±0.053	±0.057	±0.033	±0.031	±0.025	±0.022	±0.120	±0.095
425	10.12	−0.239	0.770	−0.366	−0.032	−0.448	−0.304	−0.079	0.025	0.912	1.888
	±0.30	±0.068	±0.079	±0.096	±0.103	±0.066	±0.058	±0.048	±0.041	±0.208	±0.149
435	7.58	−0.314	0.617	−0.254	−0.069	−0.549	−0.290	−0.072	−0.030	0.591	1.275
	±0.36	±0.077	±0.089	±0.107	±0.111	±0.069	±0.062	±0.051	±0.046	±0.156	±0.138
445	6.95	−0.111	0.392	−0.522	−0.060	−0.645	−0.258	−0.155	0.048	0.387	1.087
	±0.47	±0.079	±0.097	±0.115	±0.126	±0.078	±0.068	±0.062	±0.054	±0.154	±0.140
455	7.68	−0.306	0.707	−0.425	0.119	−0.570	−0.352	−0.112	0.014	0.670	1.563
	±0.55	±0.127	±0.151	±0.182	±0.203	±0.132	±0.117	±0.095	±0.090	±0.298	±0.232
465	11.58	−1.309	0.215	−0.721	−0.149	−0.847	0.124	−0.031	0.258	−0.889	2.853
	±2.14	±0.290	±0.492	±0.560	±0.978	±0.409	±0.297	±0.242	±0.136	±1.557	±1.386

have been determined by measuring a large number of τ decays and have been used to calculate cross sections for all other channels analyzed in this series of papers. The τ events were fitted twice, once to determine the expected value of beam momentum for a given beam setting, and the second time using this value as was done for all other event types. The distribution given in

TABLE V. Numbers of events and confidence levels. The columns labeled CLA and CLB refer to the confidence levels for the angular distributions and αP, respectively. There are no entries under CLA at 465 MeV/c since the coefficients are not overdetermined. The last column is the confidence level for the combination of Σ_0^+ and Σ_+^+.

	Σ^-				Σ_0^+				Σ_+^+				
p_K (MeV/c)	Events	Events after cuts	CLA (%)	CLB (%)	Events	Events after cuts	CLA (%)	CLB (%)	Events	Events after cuts	CLA (%)	CLB (%)	CL0+ (%)
225	37	30	28.4	8.3	30	17	27.5	68.5	23	18	18.4	0.8	12.5
235	144	119	19.3	3.6	74	43	35.0	44.2	95	80	87.0	3.6	<0.1
245	322	271	24.6	61.1	183	102	94.4	53.0	208	160	91.8	0.4	46.9
255	495	416	63.7	47.3	315	170	95.8	1.8	297	227	11.4	27.8	<0.1
265	682	556	44.0	23.0	409	247	19.4	16.2	474	384	35.1	25.7	60.9
275	756	618	86.1	7.0	498	294	59.5	37.1	517	410	82.2	61.8	71.7
285	817	668	68.3	36.3	550	325	54.7	86.3	586	467	42.4	10.1	69.0
295	780	649	23.2	40.8	497	288	59.1	9.0	603	490	7.4	86.9	53.1
305	652	553	67.7	50.1	442	255	12.6	23.9	485	379	15.7	62.8	46.9
315	660	544	48.8	88.1	483	295	99.1	94.4	538	431	37.6	95.1	91.0
325	846	690	53.8	40.5	606	385	22.3	38.1	677	539	99.3	69.1	96.2
335	967	824	87.8	54.5	676	431	20.5	94.9	710	567	38.9	44.4	13.0
345	782	675	1.1	19.9	613	384	61.2	74.9	585	475	4.3	62.0	14.2
355	1966	1688	37.9	74.3	1400	896	41.4	64.5	1514	1257	50.1	25.4	71.4
365	5505	4764	5.6	17.4	3703	2339	0.2	48.1	4127	3375	16.3	87.3	51.5
375	9703	8281	0.8	28.4	6341	3986	29.8	33.1	6776	5580	85.8	56.1	78.9
385	14417	12147	95.6	93.1	9105	5625	17.5	57.4	10135	8196	52.2	56.7	13.8
395	10689	8934	84.8	40.0	6857	4182	30.7	77.2	7694	6231	75.2	39.3	42.4
405	7718	6279	4.5	49.1	5091	3151	94.0	23.1	5916	4730	45.5	12.7	60.2
415	3424	2777	12.9	54.3	2397	1480	90.5	46.9	2844	2306	87.1	52.9	5.9
425	1109	889	19.8	15.1	731	446	31.6	27.1	891	747	54.9	79.6	62.5
435	673	550	52.6	76.1	515	307	8.1	78.4	628	511	97.4	31.8	91.4
445	595	475	88.7	83.8	463	294	<0.1	74.4	498	417	58.5	65.9	78.9
455	259	197	16.4	<0.1	190	127	2.1	1.4	221	187	3.2	33.7	20.7
465	34	28		58.9	39	26		23.1	41	37		4.5	2.4

Fig. 1 and Table II has been corrected as described in Ref. 9.

A consequence of using the same t for all channels is that the cross sections for all channels are statistically correlated. Let σ_i and σ_j be the cross sections for two different channels at the same momentum. It can easily be shown that the off-diagonal error matrix element corresponding to σ_i and σ_j is given by $E_{ij}=\sigma_i\sigma_j(\delta t/t)^2$, where t and δt are the path length and its uncertainty given in Table II. Those planning to use the data from this series of papers in partial-wave analyses should include these correlations, or at the very least be aware of them. Failure to include the correlations can result in assigning unjustifiable statistical significance to fluctuations in total cross section. In particular, the cross sections of all channels appear to be systematically low at 285 MeV/c. Inclusion of the correlations may be necessary to interpret this structure correctly.

The cross sections and coefficients for Σ^+ have been obtained by averaging the results of Σ_0^+ and Σ_+^+. Because α_+ is nearly zero[6] the Σ_+^+ channel contributes very little to determining B_l/A_0. The χ^2 resulting from averaging is 248 for 180 degrees of freedom, corresponding to a confidence level of 0.2%. This poor confidence level results from momenta of 235 and 255 MeV/c, which have χ^2 values of 47 and 31, respectively, for 6 degrees of freedom. If we consider only the high-statistics momenta from 355 to 425 MeV/c we obtain a χ^2 of 65 for 64 degrees of freedom, corresponding to a confidence level of 43%. Confidence levels for all momenta are given in the last column of Table V. It is also interesting to calculate the branching ratio for Σ_0^+ and Σ_+^+. We obtain $\Sigma_+^+/(\Sigma_0^+ + \Sigma_+^+) = 0.499 \pm 0.002$. This is to be compared with the world-average value 0.484 ± 0.007.[6] Our value should not be included in a world average because we have not attempted to establish that systematic uncertainties are small compared with our statistical uncertainty of 0.002. However, the good value of χ^2 for the combination of Σ_0^+ and Σ_+^+ at the high-statistics momenta, together with the adequate agreement of the branching ratio with the world-average value, provide verification of the accuracy of the large corrections that have been applied for cuts and inefficiencies.

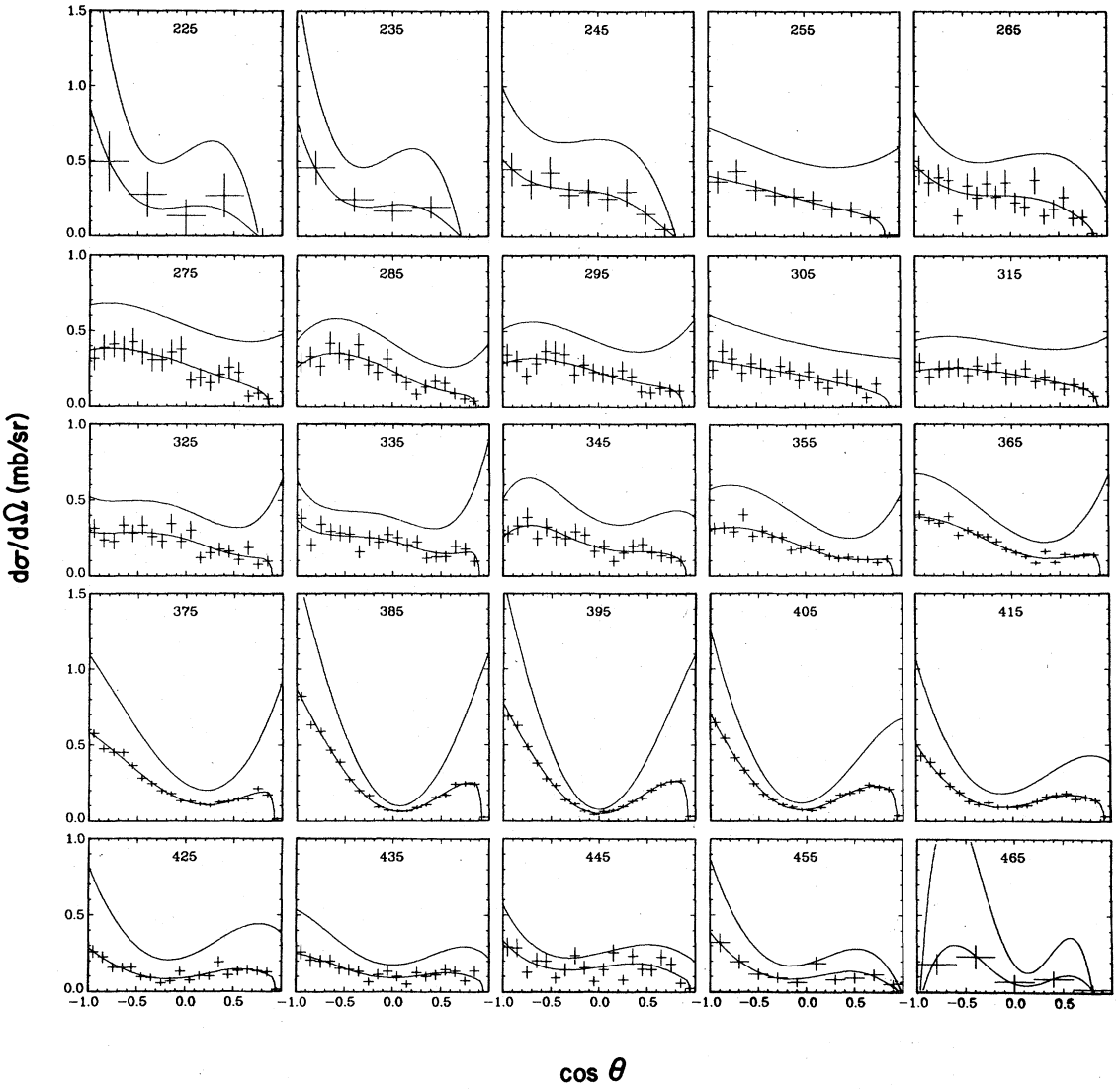

FIG. 5. Differential cross section for $\Sigma^*_0 \pi^-$ as a function of production cosine.

IV. RESULTS

The results of the fits described in Sec. III are given as a function of beam momentum, p_k in Tables III and IV. The B_l/A_0 coefficients in Table IV correspond to $\alpha_0 P$ rather than $\alpha_+ P$ or P. Note that we have included only the diagonal errors. Complete error matrices are given in a separate report.[10] Although most of the coefficients were determined using the maximum-likelihood method, we have calculated χ^2 for each fit. The confidence levels corresponding to these values of χ^2 are given in Table V. A method of least squares was used to obtain starting values for the maximum-likelihood method; however, because the final coefficients do not exactly minimize χ^2, one would expect these confidence levels to be systematically low. Nevertheless, the quality of the fits is reasonably good.

Graphic presentation of the data is given in Figs. 4 through 11. Figure 4 shows $d\sigma/d\Omega$ as a function of production cosine $(\hat{K} \cdot \hat{\pi})$ for $\Sigma^- \pi^+$. There are two solid curves for each momentum. The upper curve gives the corrected value of $d\sigma/d\Omega$, whereas the lower curve was the actual fit to the data. The data points are simply the observed (weighted) number of events scaled by the appropriate path-length factor. The lower curve is nearly equal

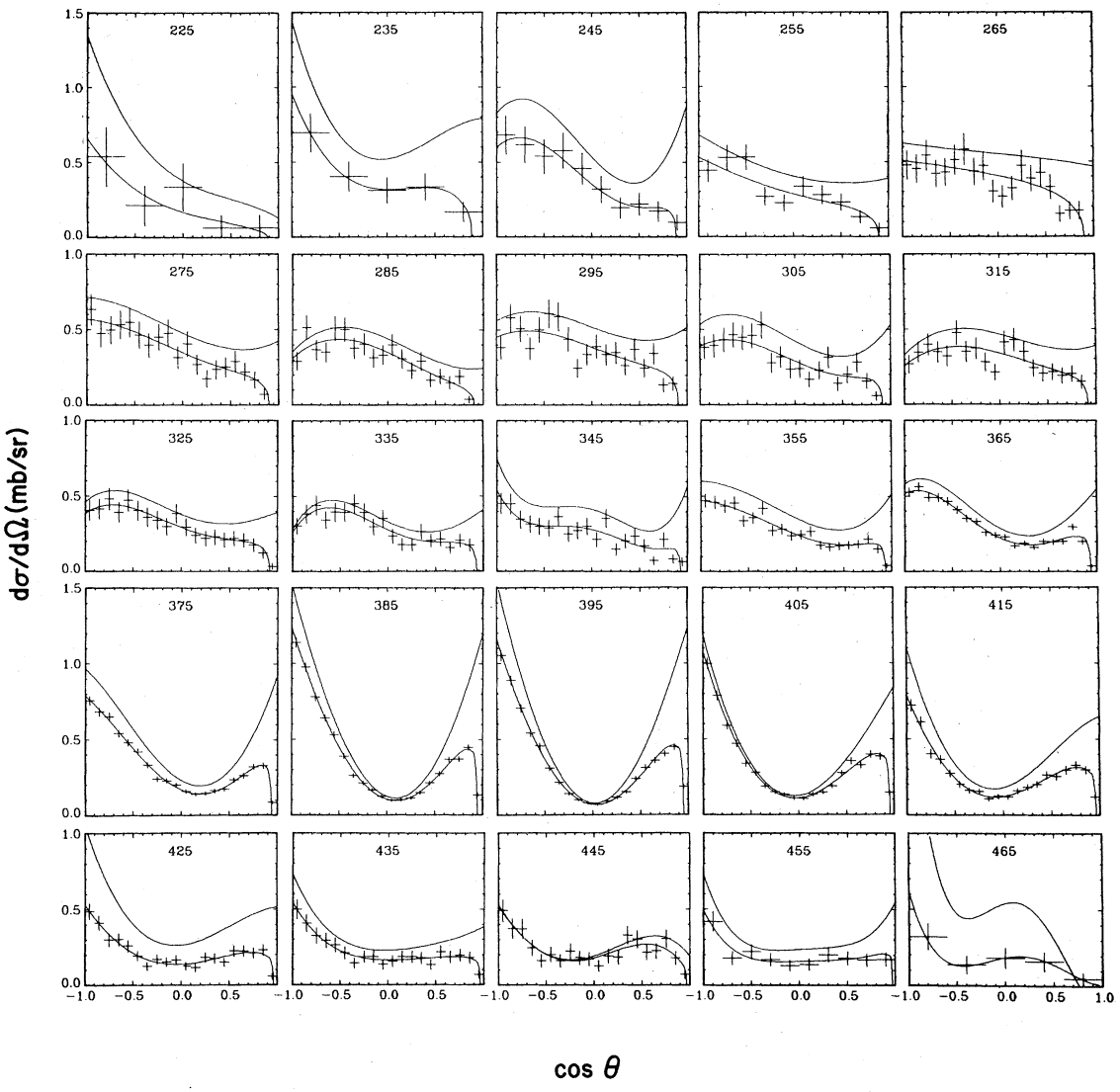

FIG. 6. Differential cross section for $\Sigma_+^+\pi^-$ as a function of production cosine.

to the survival fraction s times the upper curve. This equivalence is not exact because the upper curve includes the beam-averaging corrections described in Sec. III C. The difference in the curves dramatically illustrates the rather drastic corrections that are necessary to account for poorly visible Σ events. Figures 5 and 6 are the same as Fig. 4, but refer to the Σ_0^+ and Σ_+^+ channels.

Because there are no data, $d\sigma/d\Omega$ is poorly determined at 0° ($\cos\theta = 1$) and fluctuates rather widely. Nevertheless, in examining Figs. 5 and 6, one might suspect a bias that causes the cross sections to be systematically low at this angle. Although we believe we have been very careful in our data analysis, we cannot entirely rule out the possibility of some undetected bias. We note, however, that if such a bias does exist it is likely to be small compared with the large uncertainty in the cross section at 0°. The cross sections at both 0° and 180° are given in Fig. 7. The uncertainties for these cross sections were calculated using the full error matrices.

Figure 8 shows αP as a function of $\cos\theta$ for the $\Sigma_0^+\pi^-$ channel. The curves are calculated from the B_l/A_0 coefficients given in Table IV. The data points were obtained using the method of moments and are given by $\alpha P = \sum_{i=1}^{N} \cos\beta_i / \sum_{i=1}^{N} \cos^2\beta_i$. The data points have been corrected for the beam-averaging effects described in Sec. III C and are

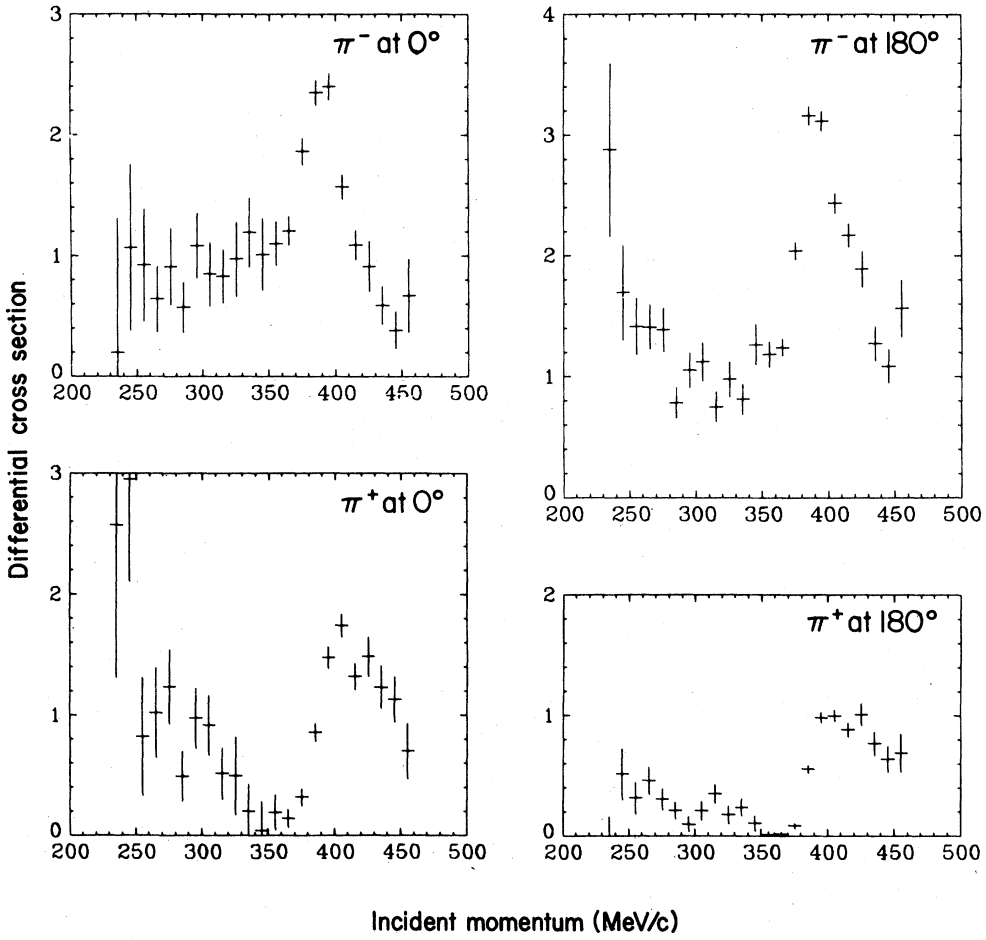

FIG. 7. Differential cross sections at 0° and 180° as a function of beam momentum for $\Sigma^- \pi^+$ and $\Sigma^+ \pi^-$.

shown simply to illustrate the quality of the fits to the data. Figure 9 shows αP as a function of $\cos\theta$ for $\Sigma^-_- \pi^+$ and $\Sigma^+_+ \pi^-$ at a single momentum, and illustrates the limited value of this information in determining B_1/A_0. The cross sections and Legendre-polynomial coefficients for Σ^- and Σ^+ are plotted in Figs. 10 and 11.

V. CONCLUSIONS

This paper completes the presentation of experimental results of a high-statistics bubble-chamber investigation of $K^- p$ reactions between 220 and 470 MeV/c. In all of the papers in this series, we have devoted special attention to reducing biases to a level that we believe is smaller than the statistical uncertainties. In particular, we addressed the difficult problem of evaluating the number of events and path length in each 10-MeV/c interval to determine that the momentum dependences of the various cross sections had been done correctly. This work therefore supersedes previous formation experiments of this type in quality and quantity.[2,11]

In the momentum region from 360 to 420 MeV/c, spanning the $\Lambda(1520)$ resonance, the path length was sufficient to yield about 5 000 to 10 000 events in each channel for every 10-MeV/c momentum interval. Above and below this region, the path lengths were typically an order of magnitude lower. Thus, the central momentum region has enough statistical precision for most strong-interaction analyses. The higher- and lower-momentum regions, especially below 270 MeV/c, still suffer from inadequate statistics. Where our results overlap those of other experiments, centered above[12] and below[13] this momentum region, good agreement is generally achieved.

Apart from the $\Lambda\pi^\circ$ reaction, all channels studied have shown the following behavior in the Leg-

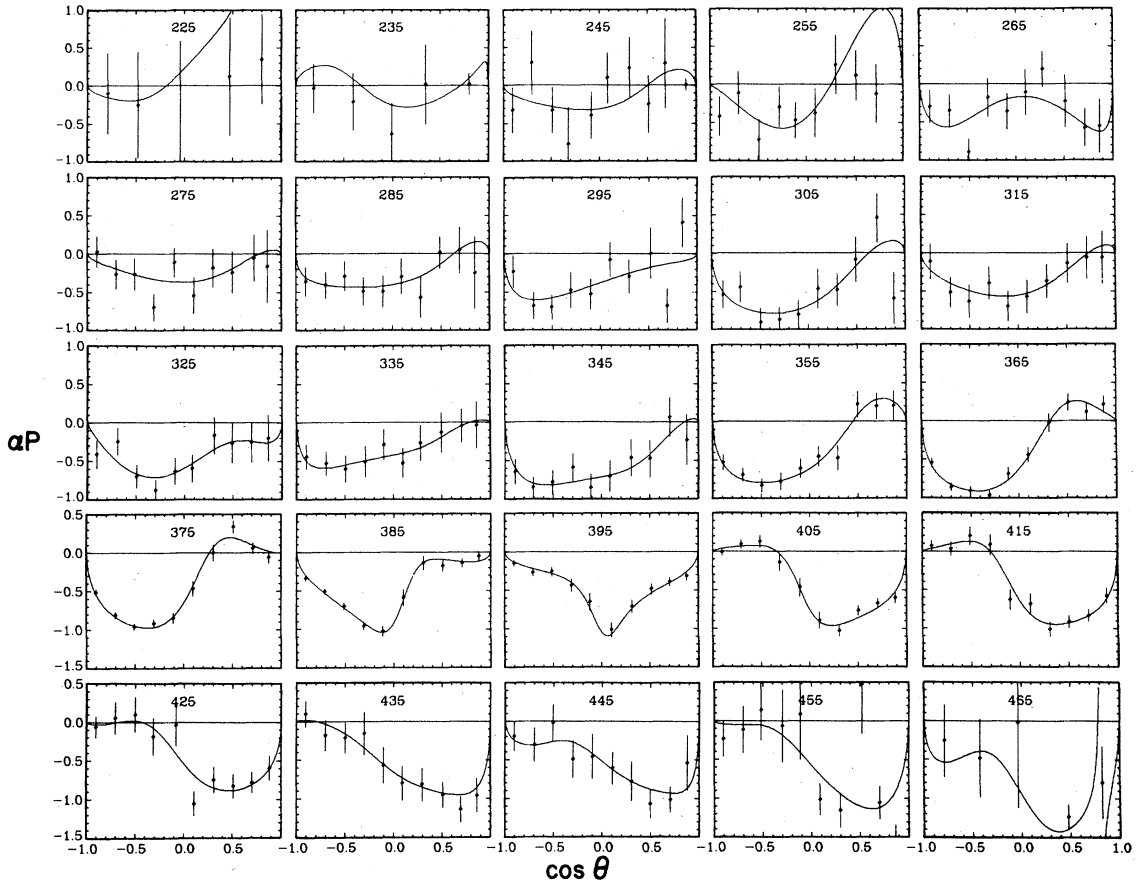

FIG. 8. Curves of αP and data as a function of $\cos\theta$ for $\Sigma_0^+\pi^-$.

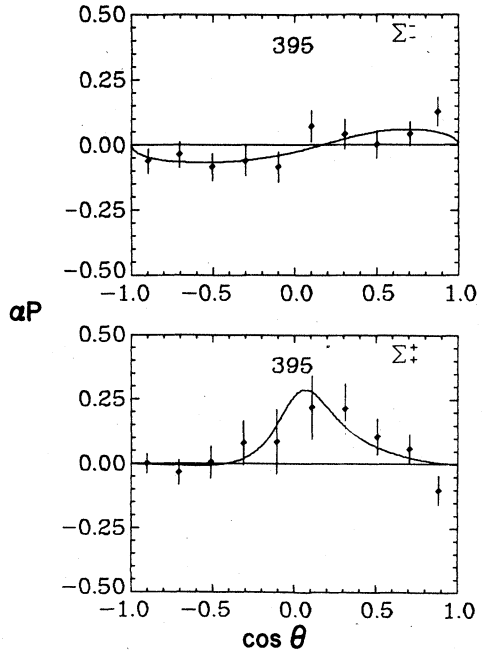

FIG. 9. Curves of αP and data as a function of $\cos\theta$ for $\Sigma_-^-\pi^+$ and $\Sigma_+^+\pi^-$ at 395 MeV/c.

endre-polynomial coefficients of the angular distributions and polarizations: (1) large even polynomial coefficients (A_0, A_2, and B_2) and relatively smaller odd coefficients (A_1, A_3, B_1, and B_3); and (2) substantial momentum-dependent structures in these coefficients in the vicinity of $\Lambda(1520)$. These structures have been adequately explained[2] by the dominance of the $\Lambda(1520)$ $D_{3/2}$ wave resonance superimposed upon a large S-wave background. A considerably smaller P-wave background is also evident from the presence of smaller odd polynomial terms in the expansions. A very small, barely significant fourth-order coefficient signals the beginnings of a $D_{5/2}$ amplitude.

There is no statistically significant evidence for structure in the data beyond that which can be understood in terms of the $\Lambda(1520)$ resonance interfering with slowly varying background amplitudes.

ACKNOWLEDGMENT

This work was supported by the High Energy Physics Division of the U.S. Department of Energy under Contract No. W-7405-ENG-48.

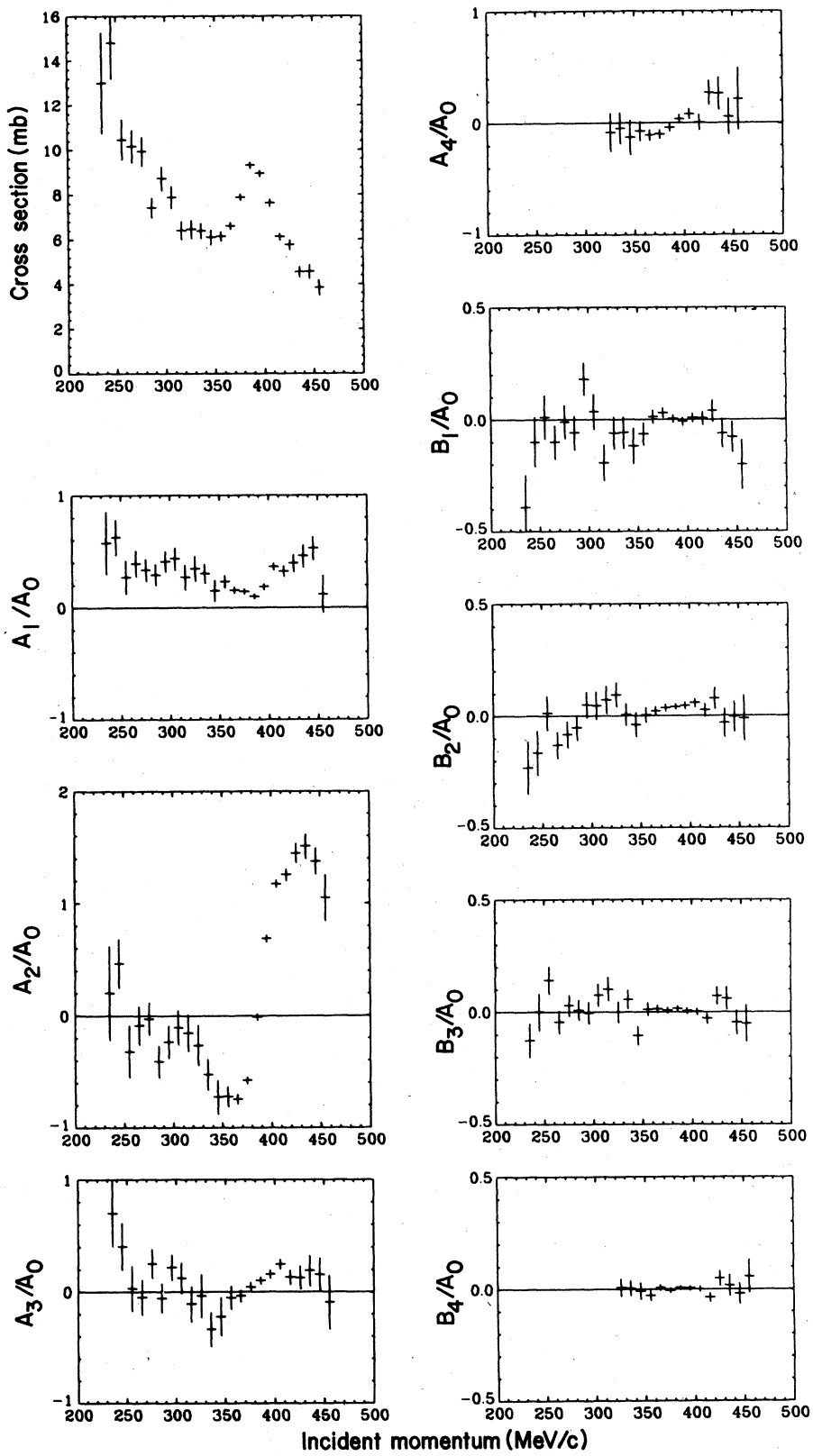

FIG. 10. Cross sections and Legendre-polynomial coefficients as a function of momentum for $\Sigma^- \pi^+$.

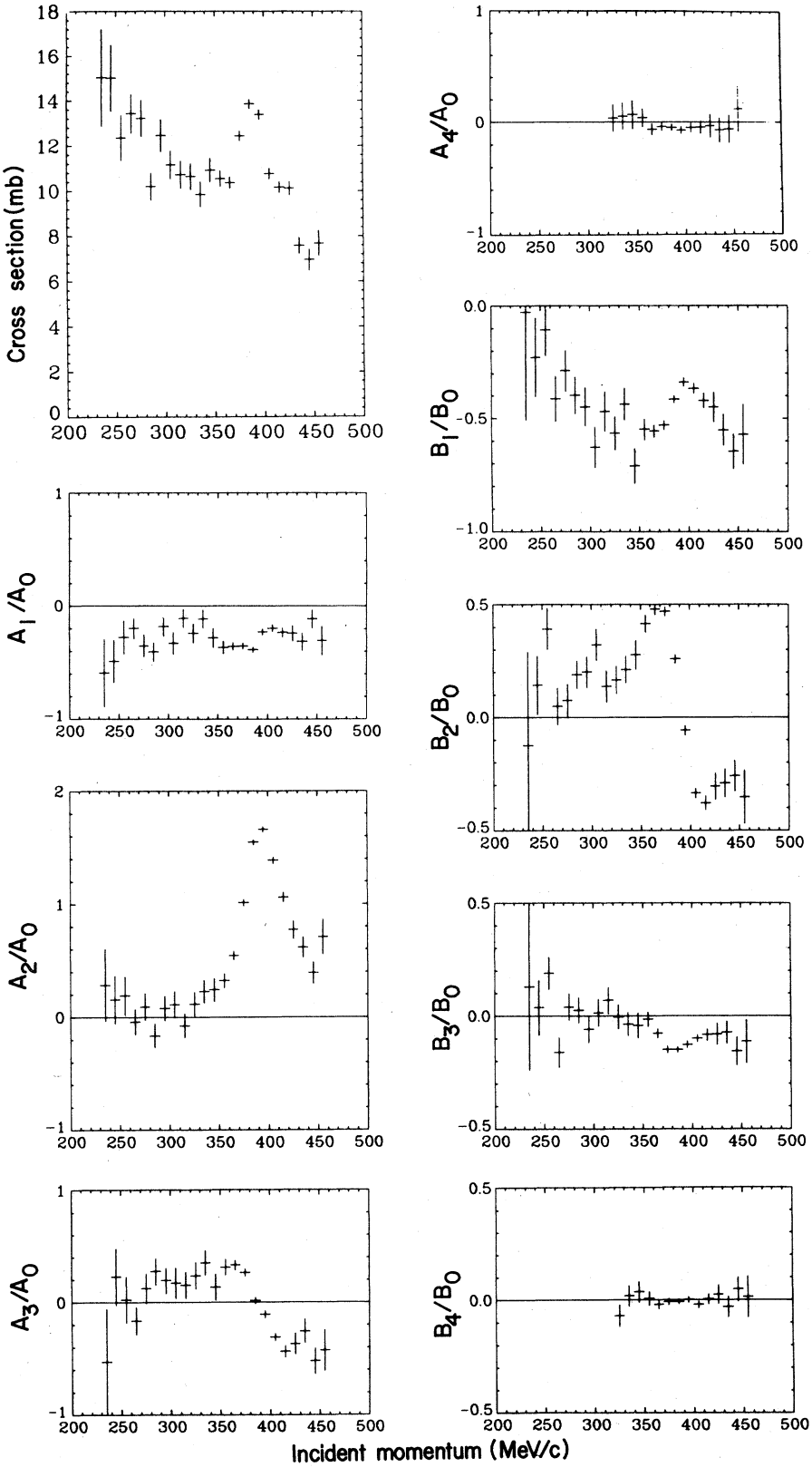

FIG. 11. Cross sections and Legendre-polynomial coefficients as a function of momentum for $\Sigma^+\pi^-$.

*Currently at Lawrence Livermore Laboratory.
[1]T. S. Mast, M. Alston-Garnjost, R. O. Bangerter, A. Barbaro-Galtieri, F. T. Solmitz, and R. D. Tripp, Phys. Rev. D 14, 13 (1976); 11, 3078 (1975); 7, 5 (1973); 7, 3212 (1973); Phys. Rev. Lett. 21, 1715 (1968).
[2]M. G. Watson, M. Ferro-Luzzi, and R. D. Tripp, Phys. Rev. 131, 2248 (1963).
[3]R. O. Bangerter, A. Barbaro-Galtieri, J. P. Berge, J. J. Murray, F. T. Solmitz, M. L. Stevenson, and R. D. Tripp, Phys. Rev. Lett. 17, 495 (1966).
[4]R. O. Bangerter, Ph.D. thesis, University of California, U.C. Radiation Laboratory Report No. UCRL-19244, 1969 (unpublished).
[5]R. O. Bangerter, M. Alston-Garnjost, A. Barbaro-Galtieri, L. K. Gershwin, T. S. Mast, J. J. Murray, F. T. Solmitz, M. L. Stevenson, and R. D. Tripp, Phys. Rev. 187, 1821 (1969).
[6]Particle Data Group, Phys. Lett. 75B, 1 (1978).
[7]S. E. Derenzo and R. H. Hildebrand, Nucl. Instrum. Methods 69, 287 (1969); R. Bangerter, Lawrence Berkeley Laboratory Group A Physics Note No. 873, 1979 (unpublished).
[8]F. T. Solmitz, Annu. Rev. Nucl. Sci. 14, 375 (1965).
[9]R. Bangerter, Lawrence Berkeley Laboratory Group A Physics Note No. 874, 1979 (unpublished).
[10]T. S. Mast and R. O. Bangerter, Lawrence Berkeley Laboratory Report No. LBL-3853 (in preparation).
[11]D. Berley, S. P. Yamin, R. R. Kofler, A. Mann, G. W. Meisner, S. S. Yamamoto, J. Thompson, and W. Willis, Phys. Rev. D 1, 1966 (1970).
[12]R. Armenteros, P. Baillon, C. Bricman, M. Ferro-Luzzi, E. Pagiola, J. O. Petersen, D. E. Plane, N. Schmitz, E. Burkhardt, H. Filthuth, E. Kluge, H. Oberlack, R. R. Ross, R. Barloutaud, P. Granet, J. Meyer, J. P. Porte, and J. Prevost, Nucl. Phys. B21, 15 (1970).
[13]J. K. Kim, Columbia University Nevis Laboratories Report No. NEVIS-149, 1966 (unpublished); M. Sakitt, T. S. Day, R. G. Glasser, N. Seeman, J. Friedman, W. E. Humphrey, and R. R. Ross, Phys. Rev. 139, B719 (1965).